

Development of an improved newtonian total radiometer, its evaluation and calibration

Rafael Castrejón-García

Instituto de Investigaciones Eléctricas

Av. Reforma 113, Col. Palmira, 62490 Temixco, Mor., Mexico

Alejandro Morales

Centro de Ciencias Físicas, Universidad Nacional Autónoma de México

P.O. Box 48-3, 62251 Cuernavaca, Mor., Mexico.

Recibido el 11 de marzo de 1998; aceptado el 24 de agosto de 1998

Measuring of radiant energy by optical non intrusive means is an important topic of research in many areas of science and technology. Precise evaluation of thermal energy emitted by hot bodies leads to a better understanding of the energy interchange phenomena between the body and its surroundings. To this end, a wide spectrum optical radiometer was developed. In this article we describe the construction and evaluation of this instrument and the physical principles involved in its design and operation. Among other advantages, the linear response of the instrument allows easily a precise calibration. Additionally, we give a procedure to obtain a known source of radiation that was used to calibrate the radiometer.

Keywords: Radiometer; thermal radiation

La medida de la radiación por medios ópticos no intrusivos es un tópico de investigación importante en muchas áreas de la ciencia y la tecnología. La evaluación precisa de la energía térmica emitida por cuerpos calientes conduce a una mejor comprensión del fenómeno de intercambio de energía entre los cuerpos y sus alrededores. Con tal propósito, se desarrolló un radiómetro óptico de amplio espectro. En este artículo describimos la construcción y evaluación de este instrumento y de los principios físicos involucrados en su diseño y funcionamiento. Entre algunas de sus ventajas se puede citar la respuesta lineal del instrumento, lo cual permite una calibración sencilla y precisa. Adicionalmente, damos un procedimiento para obtener una fuente de radiación conocida que se usa para calibrar el radiómetro.

Descriptores: Radiómetro; radiación térmica

PACS: 07.60.Dq; 42.72.Ai; 44.40.+a

1. Introduction

Thermal and optical radiation are some of the most important phenomena to transport energy in the universe. Most of the energy coming from the sun which makes earth an habitable place is transported by radiation. All bodies emit radiation in an amount that depends on their temperature and type of surface. If that ubiquity of radiation were not enough to justify its study by itself still many technological and practical uses could be mentioned to exhibit its importance.

Radiometry and its closely related area black-body radiation, are active areas of research. Cryogenic radiometers, and black-body enclosures are being used to determine with higher accuracy the Stefan-Boltzmann constant [1]. Absolute measurements of intensity of laser radiation are also benefited with those radiometric advances. Small black-body [2] cavities coupled to semiconductor light detectors by optical fiber could surpass thermocouples at very high temperature measurements.

The work described in this article was originated by the need of measuring the radiant power generated by heavy fuel oils to produce electrical energy.

The power radiated by a body increases very rapidly with its temperature, for this reason at high temperature the transfer of heat by radiation becomes larger than the transfer produced by heat conduction and convection. One example of this situation are industrial burners where the flames can reach the temperature of 2000 K, making radiation the dominant process of heat transfer. Since the amount of radiation produced in those burners depends on the emissivity and the temperature reached by the flames, the measurement of these parameters constitutes a form to evaluate the radiated power; but the direct measurement of temperatures near 2000 K is not an easy task. Moreover, the dependence of the emissivity on the composition of the flames and the lack of thermal equilibrium found therein impairs the utility of optical pyrometers [3, 4].

Those limitations are not present if the total radiated power is measured directly by a total radiometer; where by total radiated power we mean the integration of the power with independence of the wavelength. For the measurement of radiated power with a total radiometer, neither the emissivity valuation nor thermal equilibrium are required.

This article describes the development and calibration of an optical total radiometer capable of measuring the intensity

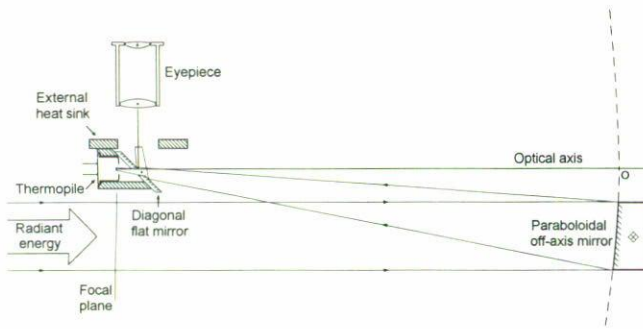


FIGURE 1. Schematic diagram of the radiometer.

of the radiation emitted by a body in the range 500–2000 K. The needed accuracy to achieve the practical goal is about 1%. According to Palmer [5], this accuracy is situated in the mid-range of the actual level of development.

The radiometer has an off-axis aluminum coated paraboloidal mirror to focus the radiation on a thin-film thermopile. The voltage produced by radiation on the thermopile was directly measured with a microvoltmeter. To show directly the radiant flux in units of W/cm^2 , a linear variable gain amplifier and an ADC (analog to digital converter) were used.

The radiation coming from a spherical furnace [6], which was heated at different temperatures was used to calibrate the radiometer. The spherical symmetry simplifies the calculations needed to evaluate the corrections relative to black-body radiation, in terms of the size of the furnace aperture. In this article we present a calibration based in that geometry.

Finally we present a discussion of the global accuracy of the instrument and the results of monitoring a flame with the radiometer.

2. Optics and detector thermopile layout

The radiometer has a paraboloidal mirror (PM) in Herschel mount to collect and focus the radiation on a thin-film thermopile (T) that works as the radiation detector. A diagonal mirror used as in the newtonian complement, directs some light to an eyepiece to aim the instrument toward the hot body. This configuration warrants an enough wide spectrum collection to pick-up most of the radiation emitted by bodies up to 2000 K. The limited spectral window of other kind of radiation detectors and the strong absorption bands of the materials which lenses are made, make them not well adapted to collect all of the radiation produced by bodies up to 2000 K; in contrast, thermopiles and aluminum coated mirrors have a good response in most of the wavelength range of radiation emitted by hot bodies. The absence of chromatic aberration for reflective optics is also a decisive advantage, specially if a wide radiation spectrum response in the instrument has been considered.

Though thermopiles are not the most sensitive detectors, they respond linearly to optical power. The spatial non-uni-

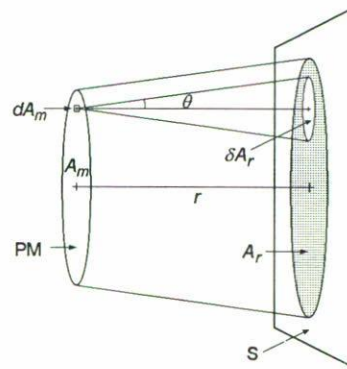


FIGURE 2. Important rays to define the optical input of the radiometer.

formities reported by Theocharous, Fox and Prior [7] for this kind of detector, are not important in our case due to the calibration procedure.

Figure 1 shows a diagram of the elements of the radiometer. The radiation coming from the hot body is focused on the T by the off-axis aluminum coated PM. The mirror which has a circular cross section relative to the optical axis, with a diameter of 20 mm, was polished at the optical workshop of the Instituto de Astronomía, UNAM. To aim the instrument toward the hot body, the flat diagonal mirror directs a small amount of light to the eyepiece. The hole in this mirror is ample enough to assure that the radiant power input of the system is only related to the dimensions of the PM and the T. The radiation passing through the hole of the flat mirror is concentrated on the surface of T. The thermopile with a flat optical response, has a sensitive surface with a diameter of 1 mm; this surface is located to be coincident with the focal plane of the mirror, and centered with the optical axis of the PM. The sensitive surface defines the internal border of the field stop of the system.

The T is attached to the external heat sink, which makes thermal contact with the thermopile heat sink, as shown in Fig. 1.

Since the sensitive surface of the T is located on the focal plane, its image is at infinity with its circular border subtending an angle $\theta \simeq 0.19^\circ$ with respect to the optical axis. This angle was calculated for a radius of the T of 0.5 mm and a focal length of 150 mm for the PM. Then the field of view is $\theta_{\text{view}} = 2\theta = 0.38^\circ$ because any ray touching the mirror and making an angle less than 0.19° with the optical axis will reach the T.

The important rays which define the entrance characteristics of the instrument are shown in Fig. 2. The PM is represented as flat with area A_m ; S is a radiant surface. The sides of the truncated cone that starts on the PM make an angle θ with the optical axis. That cone intersects the surface S which is at the distance r , in a circular surface with area A_r . Incident rays on points outside area A_r cannot reach the surface of the thermopile. The area dA_m contains the vertex of other cone whose sides make also an angle θ with

the optical axis, and intersect surface S in a circle of area $\delta A_r = \pi r^2 \tan^2 \theta$, where θ is considered as a very small angle. In terms of the solid angle subtended by the surface δA_r we have $\Omega = \pi \tan^2 \theta$.

Assuming that surfaces A_m and A_r are perpendicular to r , then the power radiated from area δA_r to dA_m is,

$$q_{\delta A_r \rightarrow dA_m} = i_r \frac{\delta A_r dA_m}{r^2}, \quad (1)$$

where i_r is the intensity of radiation emitted by δA_r . (i_r corresponds to L_e , the radiance, in the Wolfe [8] nomenclature).

By construction, all the rays starting at δA_r and ending in dA_m will reach the thermopile, then the integration over the area dA_m will give the total power entering the radiometer. To each differential area dA_m in there corresponds an area δA_r in A_r . Although to two adjacent differential areas in A_m correspond two partially superposed areas δA_r on A_r , no ray is counted twice, since every ray is associated to a unique differential area in A_m . From this consideration the total power entering the instrument is obtained by integrating $q_{\delta A_r \rightarrow dA_m}$ over A_m in Eq. (1):

$$q_{A_r \rightarrow A_m} = i_r \int_{A_m} \frac{\pi r^2 \tan^2 \theta dA_m}{r^2} = \pi i_r \tan^2 \theta A_m. \quad (2)$$

For isotropic radiation the hemispherical density of radiant flux is $\Phi_r = \pi i_r$. (Φ_r corresponds to M_e , the radiant exitance, in the Wolfe [8] nomenclature). Introducing this magnitud and Ω in Eq. (2) we get

$$q_{A_r \rightarrow A_m} = \frac{\Omega A_m}{\pi} \Phi_r. \quad (3)$$

The previous equation relates the instrumental parameters Ω and A_m to the measurement of Φ_r in terms of $q_{A_r \rightarrow A_m}$. It also shows the independence of the measurement with the distance r assuming that all the area A_r can be seen by the instrument. Since angle θ is small, A_r does not increase very rapidly with the distance, allowing this fact a long range of measurements for small areas.

Paraboloidal mirrors have null spherical aberration for images in the focal plane but off-axis images have astigmatism and coma. Considering a f -number of $f/7.5$ and a position of 0.5 mm off axis, it corresponds a saggital coma and astigmatism [9] of 5.5×10^{-4} mm and 1.1×10^{-4} mm, respectively. Assuming as an upper bound the addition of these two magnitudes, we have a total aberration of 6.6×10^{-4} mm. This number is near to the radius of the first dark ring of the Airy pattern calculated for the radiometer [10] 4.0×10^{-4} mm, for the smallest of the wavelengths involved $\lambda = 0.2 \mu\text{m}$. For this reason the radiometer can be considered as diffraction-limited in the sense that the border of the monitored area is mainly defined by diffraction. However in terms of optical power, diffraction can be neglected because power lost by points inside Ω (because some of the power does not reach the thermopile), is compensated by the power gained by points outside Ω . Then, total aberration is the only

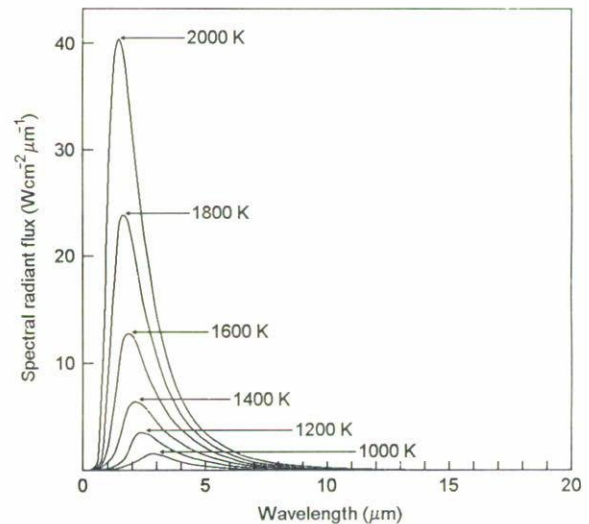


FIGURE 3. The Planck's distribution curves.

remaining effect that modifies the constant factor of Eq. (3). Since aberration is independent of wavelength, Eq. (3) maintains its linearity, therefore, calibration will correct the small aberration factor. For a thermopile radius of 0.5 mm and a total aberration of 6.6×10^{-4} mm, this factor is $\approx 0.3\%$ (this factor is the ratio of the aberration area and the T area).

3. Black-body furnace theory and radiometer calibration

The Planck distribution curve [11] gives, in terms of the wavelength, the radiant flux per unit wavelength (spectral radiant flux), radiated by an ideal black-body at temperature T , as shown in Fig. 3. The integration of this radiant flux over all wavelengths from $\lambda = 0$ to infinity, gives the total emitted power per unit area by the black-body at that temperature (total black-body radiant flux). According to Stefan-Boltzman law this radiant flux is $\Phi_B(T) = \sigma T^4$, where σ is the Stefan-Boltzman constant. Then, to calibrate the radiometer, a black-body furnace is used as a source of known radiant flux at all wavelengths.

Two points arise in relation to the calibration process:

- To get a near black-body radiation, radiant power is supplied by a furnace with a small hole on its wall. This hole slightly modifies the radiation equilibrium as compared with a perfect closed furnace and consequently a correction must be made to consider this radiation leak. This correction is discussed later in this section.
- It is necessary to consider the fraction of the total power lost by absorption in the paraboloidal mirror and reflection in the thermopile. However, if absorption in the mirror or reflection in the thermopile are not dependent of the wavelength, they do not degrade the performance of the instrument, because these losses can be corrected by calibration.

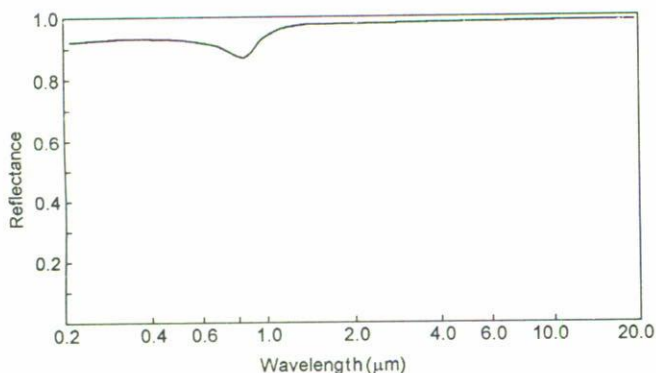


FIGURE 4. Curve of aluminum reflectance.

Aluminum is the material with maximum reflectivity in the range from 0.2–20 μm. Figure 4, shows the reflectivity of aluminum in that wavelength range as reported in the Handbook of Optics [12]. Bennet, Silver and Ashley [13], measured the same reflectivity including longer wavelength. They showed that for longer wavelengths the reflectivity increases monotonically almost up to 0.99 for 40 μm. The amount of radiated power outside the 0.2–40 μm range for a temperature of 2000 K is smaller than 0.08 %. Or 0.18 % in the range 0.2–20 μm; for a tabulation of the integral of the Planck distribution with respect to the wavelength for different temperatures see Refs. 18 and 19.

The small depression in the curve near 0.9 μm is far from the maximum for most of the radiation curves of Fig. 3 (at 1800 K the peak is on ~ 1.6 μm), therefore, a small loss of linearity would be expected at higher than 1600 K temperatures. Nevertheless, the effect on the linearity caused for that depression is evaluated in Sect. 5, by recording the response of the instrument at different temperatures. Similarly, variations in the absorbance of the thermopile would be detected in the same recording.

Returning the discussion to point a), it is important to say that spherical enclosure is an attractive design because the mathematical problem it poses can be solved easily in a closed form for a gray, Lambertian and isothermal surface. Other geometries [14], more convenient from the point of view of cost, dimension or accuracy, must be solved by analytical [15, 16] or numerical methods [17]. For 1% accuracy required in this work the spherical cavity is an excellent option.

Figure 5 shows the principal elements of the spherical furnace used to calibrate the radiometer. The cavity radius is 150 mm and the radius of the hole is 12.5 mm; this radius was made to be greater than the field of view of the radiometer. The internal wall is a single piece moulded with high alumina cement, 25 mm width. A stopper of the same material blocks the hole when the furnace is in the heating process. On the wall external surface a kantal resistor is inserted into a groove and all the surface is covered with high temperature cement. The space between the external metallic container and the cement is filled with thermal insulator. A type R thermocouple is used to measure the furnace temperature.

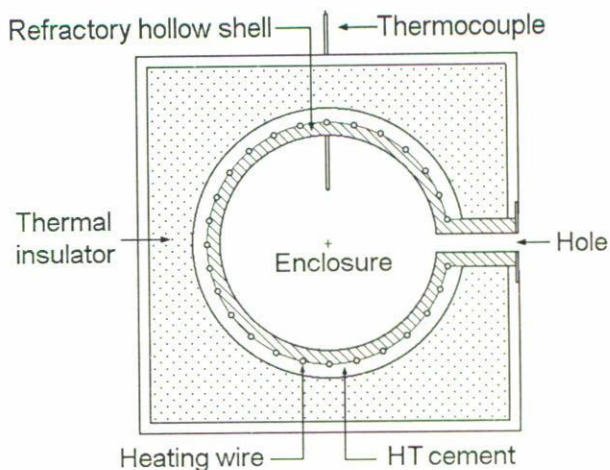


FIGURE 5. Elements and structure of the black-body furnace.

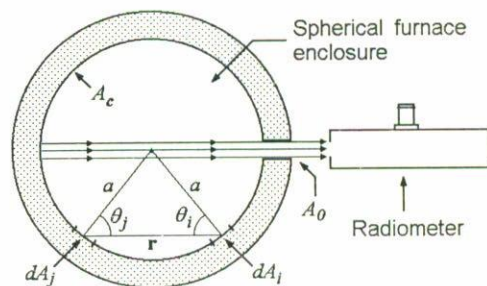


FIGURE 6. Illustration of the relative position of the black-body furnace and the radiometer.

The diffuse configuration factor [18, 19] between surfaces dA_i and dA_j is, (see Fig. 6):

$$dF_{dA_i \rightarrow dA_j} = \frac{q_{dA_i \rightarrow dA_j}}{q_{dA_i \rightarrow \cap}}, \tag{4}$$

where $q_{dA_i \rightarrow dA_j}$ is the radiant flux going from dA_i to dA_j and $q_{dA_i \rightarrow \cap}$ is the hemispherical flux leaving dA_i . In terms of W_i the hemispherical density of radiant flux leaving the surface dA_i , we have

$$q_{dA_i \rightarrow dA_j} = dF_{dA_i \rightarrow dA_j} dA_i W_i. \tag{5}$$

It is well known, that due to the spherical symmetry of the enclosure, the diffuse configuration factor associated to the area dA_i is not dependent on the position of the element dA_i (see Refs. 18 and 19). For a the radius of the enclosure, this factor is

$$dF_{dA_i \rightarrow dA_j} = \frac{dA_j}{4\pi a^2}. \tag{6}$$

The hemispherical radiant flux W_j leaving the surface dA_j assumed as gray, lambertian, diffuse and opaque is

$$W_j = \epsilon_j \Phi_B + (1 - \epsilon_j) H_j, \tag{7}$$

where ϵ_j and $1 - \epsilon_j$ are the surface emissivity and reflectivity of the internal walls of the furnace, respectively. Φ_B

is the hemispherical radiant flux for a black-body and H_j is the radiant flux coming from the remaining elements of the enclosure area. The first term in the right side of Eq. (7) is the radiation emitted, which is associated to the temperature of the surface (self-radiation) and the second is the radiation reflected by the same surface according to Kirchoff's law.

Since the radiation in an enclosure with thermodynamical equilibrium is isotropic, then $W_j = H_j$. Introducing this fact in Eq. (7), we get $W_j = H_j = \Phi_B$ as expected even in the case where the wall is not a black surface ($\epsilon_j < 1$).

If the enclosure has a small hole with area A_0 , then $H_j < W_j$ because the contribution of the hole is excluded (assuming that no radiation is entering through the hole).

For this case H_j can be calculated from Eq. (6) as

$$H_j = \frac{1}{dA_j} \int_{A-A_0} dF_{dA_i \rightarrow dA_j} dA_i W_i, \quad (8)$$

where A is the internal area of the furnace.

Introducing the configuration factor from Eq. (6) in the last integral and taking W_i constant as it corresponds to spherical symmetry and thermal equilibrium (isothermal walls), we have

$$H_j = \frac{A - A_0}{4\pi a^2} W_i = \left(1 - \frac{A_0}{4\pi a^2}\right) W_i. \quad (9)$$

Again, since $W_i = W_j$, from Eqs. (7) and (9) we have

$$W_j = \frac{\Phi_B}{1 + \left(\frac{1}{\epsilon_j} - 1\right) \frac{A_0}{4\pi a^2}}. \quad (10)$$

Since H_j is the density of radiant flux coming from the whole internal surface of the furnace, this density is also the hemispherical radiant flux escaping through the hole. Then, the hole can be considered as a radiant imaginary surface with a density of hemispherical radiant flux obtained from Eqs. (9) and (10) as

$$H_j = \frac{\left(1 - \frac{A_0}{4\pi a^2}\right) \Phi_B}{1 + \left(\frac{1}{\epsilon_j} - 1\right) \frac{A_0}{4\pi a^2}}. \quad (11)$$

The last equation shows that in the limit when $A_0 \rightarrow 0$, the radiation from the hole approximates the black-body radiation independently of the emissivity of the walls. The term $A_0/4\pi a^2$ which quantifies the proximity to the black-body radiation is named "cold fraction".

Equation (11) gives the amount of radiation emitted hemispherically by the hole (solid angle of 2π sr). When the radiometer is aimed to the furnace it collects only an unidirectional beam of radiation coming from the bottom of the internal surface, as can be seen in Fig. 6. Eq. (3) gives the amount of radiant power $q_{A_r \rightarrow A_m}$ collected by the radiometer

in terms of Φ_r . Identifying Φ_r with W_j in Eq. (10) we have

$$q_{A_r \rightarrow A_m} = \frac{\Omega A_m}{\pi} \frac{\Phi_B}{1 + \left(\frac{1}{\epsilon_j} - 1\right) \frac{A_0}{4\pi a^2}}. \quad (12)$$

This last equation quantifies the amount of radiant power falling on the thermopile in terms of known parameters when the radiometer is aimed to the calibrating black-body furnace.

Hottel's [20] equations for hemispherical and unidirectional emissivities of the hole, $\epsilon_{2\pi}$ and ϵ_{unid} , can be derived from Eqs (11) and (12). They are:

$$\begin{aligned} \epsilon_{2\pi} &= \frac{\left(1 - \frac{A_0}{4\pi a^2}\right)}{1 + \left(\frac{1}{\epsilon_j} - 1\right) \frac{A_0}{4\pi a^2}} \\ \epsilon_{\text{unid}} &= \frac{1}{1 + \left(\frac{1}{\epsilon_j} - 1\right) \frac{A_0}{4\pi a^2}}. \end{aligned} \quad (13)$$

According to Cabannes [21] in the range of temperatures from 500 to 2000 K, the emissivity for high alumina is $0.32 \geq \epsilon_j \geq 0.18$. Substituting all data in Eq. (13) we get: $0.9922 \geq \epsilon_{\text{unid}} \geq 0.9963$. Then the emissivity of the furnace can be expressed as: $\epsilon_{\text{unid}} = 0.994 \pm 0.002$.

To take into account any loss (absorption in the PM and reflection in the T), we define the constant factor K . Then, including both K and ϵ_{unid} in Eq. (12), we have

$$q_{A_r \rightarrow A_m} = 0.994K \frac{\Omega A_m}{\pi} \Phi_B.$$

The thermopile interacts with two independent surroundings, one defined by the furnace seen through the paraboloidal mirror and the other defined by the remaining surfaces which are, as the thermopile support, to room temperature. Between the sensitive area of the T and the furnace there is thermal equilibrium only when the furnace is at room temperature. When the furnace is not at room temperature the net power Δq gained by the thermopile, is the difference between the power q radiated by the thermopile in the furnace direction, and the power received by the thermopile $q_{A_r \rightarrow A_m}$ from the furnace. With the furnace at room temperature there is thermal equilibrium, therefore we have (neglecting self-radiation of the mirror):

$$\Delta q = q_{A_r \rightarrow A_m} - q = 0.994K \frac{\Omega A_m}{\pi} \Phi_B(300 \text{ K}) - q = 0;$$

then:

$$q = 0.994K \frac{\Omega A_m}{\pi} \Phi_B(300 \text{ K}).$$

With the substitution of q with $\Phi_B(300 \text{ K}) = 0.05 \text{ W/cm}^2$ in previous equation, we get:

$$\Delta q = 0.994K \frac{\Omega A_m}{\pi} (\Phi_B - 0.05). \quad (14)$$

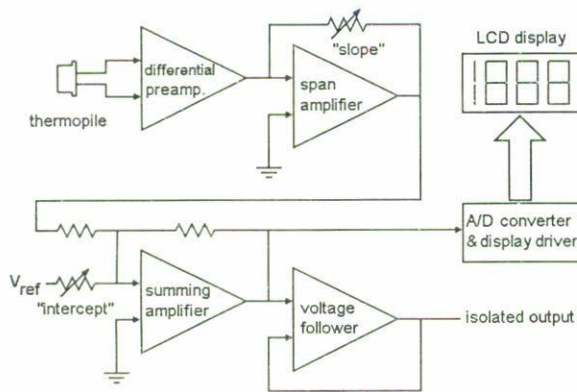


FIGURE 7. Block diagram of the electronics circuit.

Owing to the high sensitivity of the T, the self-radiation term of the T (0.05), can be considered as a constant since the increment of the temperature of the T is too small to change this term.

For a thermopile detector the responsivity [22] is $R_d = \Delta V / \Delta q$, where ΔV is the thermoelectric potential difference generated by the heating of the T. As discussed in Ref. 22 R_d is a constant that depends on detector parameters. In other words, ΔV depends linearly on Δq . From the definition of R_d we get

$$\Delta V = 0.994 R_d K \frac{\Omega A_m}{\pi} (\Phi_B - 0.05). \quad (15)$$

Due to Peltier cooling the responsivity decreases when electrical current through the junction increases. Since a high impedance microvoltmeter was used to measure the thermoelectric potential, the responsivity is maximum and corresponds to open circuit responsivity (see Ref. 22).

We are interested in measuring the radiant flux Φ_r from a hot body, therefore we define the radiometer flux responsivity as: $R_r = \Delta V / \Delta \Phi_r$, (Note the difference with the radiometer responsivity R_Φ defined by Zissis [23]). For the black-body furnace $\Phi_r = 0.994 \Phi_B$; using Eq. (15) and approximating 0.994×0.05 by 0.05, $\Delta V = R_d K \Omega A_m (0.994 \Phi_B - 0.05) / \pi$ is obtained. Then $R_r = K R_d \Omega A_m / \pi$. Finally we get:

$$\Delta V = R_r [0.994 \Phi_B(T) - 0.05], \quad (16)$$

where the dependence of Φ_B with the temperature T is stated explicitly.

Equation (16) shows the linear relation between ΔV and $\Phi_B(T)$ which allows calibration of the instrument.

4. The electronics circuitry

In order to process the electrical signal supplied by the T and considering the linear response of both the optics and the thermopile, an electronic circuit has been constructed. Figure 7 shows a block diagram of this circuit which performs the following functions:

- i) Low noise conditioning and linear amplifying of the thermoelectric signal.
- ii) Zero and span settings to furnish the radiometer calibration.
- iii) Analog to digital conversion to provide direct digital readout in radiant flux units.

As can be observed, the electronics applies over the thermopile signal a straight line function of the form:

$$E = m \Delta V + b, \quad (17)$$

with slope m and intercept b , that can be adjusted with the variable resistors: "slope" and "intercept". E is the value displayed by the LCD (Liquid Crystal Display).

According with Eq. (16), when the furnace is at room temperature $\Delta V = 0$, then the offset b is set to $b = 0.05$ to read in the LCD display a 0.05 value. Next, for an arbitrary selected value of the temperature (for instance T_s) of the furnace when the radiant flux is $0.994 \Phi_B(T_s)$, m is adjusted to get $E = 0.994 \Phi_B(T_s)$. Using this value, b and ΔV of Eq. (16) with $T = T_s$ in Eq. (17) we get $m = 1/R_r$. When this value of m and the general value of ΔV in Eq. (16) are substituted in Eq. (17) we get:

$$E = 0.994 \Phi_B(T),$$

which demonstrates that the LCD display will show the actual value of $0.994 \Phi_B(T)$.

5. Results and discussion

To get Eq. (16) it was assumed that there is no dependence of any parameter on the wavelength. As mentioned, dependence on the wavelength can arise at the mirror, the thermopile and the internal surface of the furnace (through de variation of the spectral emissivity of the wall).

To calibrate the radiometer it must be aimed to the furnace, then, the radiation travels from the furnace to the thermopile through the atmosphere. In the range from $0.2 \mu\text{m}$ to $30 \mu\text{m}$ there are important absorption molecular bands present in air, mainly due to H_2O and CO_2 . This absorption is strongly wavelength dependent. For a 0.50 cm air path length between de furnace and the thermopile, almost all spectral transmittance for these molecules in air is greater than 0.995, but some portions have a ≈ 0.9 transmittance (to standard model atmosphere), as can be estimated from the LaRocca [24] review. The relative importance of these portions is defined by its distance from the maximum of the Planck's curve; in this sense the water bands between $1 \mu\text{m}$ and $3 \mu\text{m}$ are the most important. When doing the calibration, the maximum of the Planck's curve is displaced in the range from $2 \mu\text{m}$ to $4 \mu\text{m}$; then, the importance of that absorption bands would be revealed by a non-linearity in the data.

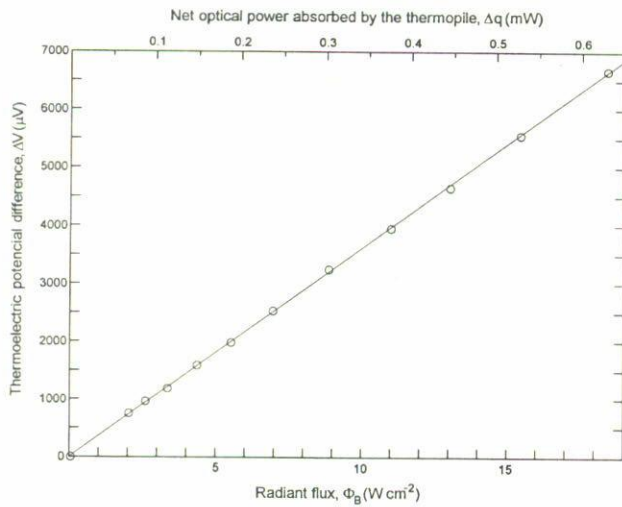


FIGURE 8. Calibration data of the radiometer.

TABLE I. Calibration data of the radiometer

Furnace Temperature (K)	$\Phi_B = \sigma T^4$ (W/cm ²)	Thermopile Potencial (μ V)	Non-linear Error (W/cm ²)	Δq (mW)
303.00	0.05	0	0.053	0
774.15	2.04	751	-0.041	0.07
823.65	2.61	963	-0.06	0.09
877.45	3.36	1185	0.08	0.11
936.85	4.37	1587	-0.03	0.15
993.85	5.53	1980	0.039	0.19
1052.65	6.96	2530	-0.049	0.24
1118.37	8.87	3246	-0.13	0.30
1180.15	11.00	3952	0.044	0.38
1231.15	13.03	4651	0.13	0.45
1284.55	15.44	5553	0.046	0.53
1342.55	18.42	6672	-0.074	0.63

Figure 8 shows the calibration data in Table I. These data correspond to a 11 days of calibration tests, since a 24 hours period between power changes was used to reach thermal equilibrium at the furnace. The thermopile voltage was directly measured by a Keithley 177 microvoltmeter. Δq column shows the optical power absorbed by the thermopile, calculated with Eq. (14), and the approximation $0.994K = 1$.

Φ_B is tabulated to test linearity with respect to the potential. The correlation coefficient between these two variables is 0.9999; which shows that the proposed linearity is correct. The non-linear error column shows the error of Φ_B with respect to the straight line produced by a linear least squares fitting with the potential. The sample standard deviation of the non-linear error data corresponds to $s = 0.076 \text{ W/cm}^2$. This last can be considered as the non-linearity error.

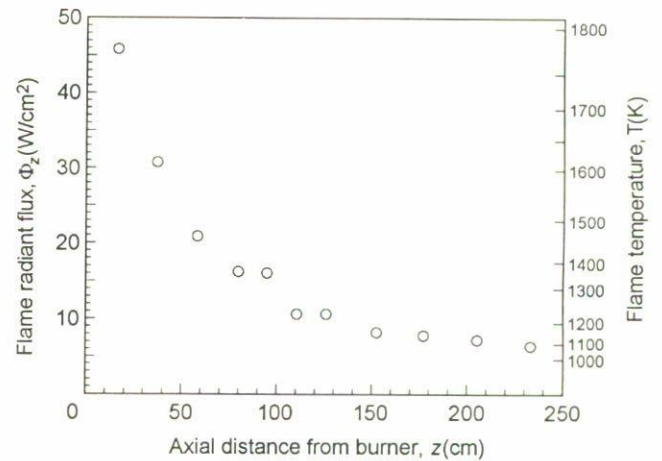


FIGURE 9. Radiant flux monitoring of a flame.

From data in Table I, the detector responsivity results: $R_d = 10.5 \text{ V/W}$, and the radiometer responsivity is: $R_r = 361.3 \pm 2.3 \mu\text{Vcm}^2/\text{W}$ (with $\Phi_r = 0.994\Phi_B$).

From data in Table I it is not possible to find a non-linear structure. One can say that all the possible non-linearities discussed previously are included in the data error structure but they are not discernible from it.

Two sources of error still not considered are the furnace temperature and thermopile Δq measurements. The accuracy of the latter is not important, since the only requirements needed are sensibility, linearity and reproducibility. By the contrary the furnace temperature is determinant. Since the platinum-rhodium thermocouple used to measure the furnace temperature has a $\pm 0.1\%$ temperature accuracy [25], the corresponding uncertainty for Φ_B is $\pm 0.4\%$. The thermocouple is near the center of the furnace, therefore the measured temperature is an average of the internal wall temperatures. For the case of low emissivity walls, which is our case, the central is the recommended position of the thermocouple since the emerging radiation is also an average. Note that in the work of Sapritsky (Ref. 17), it is concluded that the area observed by the radiometer is dominant with respect to the temperature, but that is so because they use a high wall emissivity of 0.8 (ours is 0.32–0.18).

In order to evaluate the total error of the radiometer, it is necessary to consider both, the non-linearity and the thermocouple sources of error. The best way to do this is to report both independently. Then, the non-linearity error is $s = 0.076 \text{ W/cm}^2$, and the possible error originated in the calibration by the furnace temperature uncertainty is 0.4%.

To determine the radiant flux coming from a hot body in terms of the thermopile potential, data in Φ_B column must be multiplied by 0.994. This is correct even in the case when the radiation from the hot body is not black body radiation, since the radiometer is actually calibrated. If instead of using a linear interpolation a direct reading is preferred, the ADC can be calibrated as described in Sect. 4, to show in the display the radiant flux in units of W/cm^2 .

As indicated at the beginning of this article, the radiometer was constructed to measure the total radiation of heavy fuel oils. Figure 9 shows the result of monitoring the radiant flux coming from a flame, for different positions of the radiometer. The scale at the right of the figure shows the temperature for an estimated flame's emissivity of 0.8. It must be noted that the maximum temperature (1782 K) in this scale is greater than the maximum calibration temperature (1342.55 K), owing this fact to the greater value of the black-body emissivity.

We have described the development, evaluation and calibration of a wide spectrum optical radiometer. We found it

as a powerful tool not only for the precise measurement of radiant flux, but also for the study of the radiation properties of high temperature bodies, or the determination of radiation constants of surfaces like emissivity or absorptivity. Its highly linear response allows an easy and precise calibration in a way that it can be considered as a secondary standard of calibration for instruments of its kind.

Acknowledgments

This work was partially supported by CONACyT, México, P. 1095P-E

1. J.E. Martin, *Proc. SPIE* **2815** (1996) 11.
2. T. Hisamatsu, N. Mori, T. Hamamatsu, and T. Abe, *Yokosuka Research Laboratory*, CRIEPI Rep. No. EW88005. Kanagawa, Japan, (1990).
3. V.J. Lyons and C.M. Gracia-Salcedo, *Determination of Combustion Gas Temperatures by Infrared Radiometry in Sooting and Non-sooting Flames*. NASA Technical Paper 2900, AD-A205 373. September (1989).
4. *Omega Complete Temperature Measurement Handbook and Encyclopedia*, (Omega Engineering, Inc., Stamford, 1992) Vol. 28.
5. J.M. Palmer, *Proc. SPIE* **2269** (1994) 592.
6. J.J. Velázquez-Saavedra, F. Hernández-Varela y R. Castrejón-García, *Boletín IIE*, Vol. 10, No. 6. Cuernavaca, México, (1986).
7. E. Theocharous, N.P. Fox, and T.R. Prior, *Proc. SPIE* **2815** (1996) 56.
8. W.L. Wolfe in "Radiation theory", *The infrared handbook*, edited by W.L. Wolfe and G.J. Zissis, (ERIM, Ann Arbor, 1985).
9. W.J. Smith in "Optical elements, lenses and mirrors", *The infrared handbook*, edited by W.L. Wolfe and G.J. Zissis, (ERIM, Ann Arbor, 1985).
10. W.J. Smith, *Modern optical Engineering*, Second Edition, (McGraw Hill, New York, 1990).
11. J. Kestin and J.R. Dorfman, *A Course in Statistical Thermodynamics*, (Academic Press, New York, 1971).
12. W.G. Driscoll and W. Vaughan, Eds. *Handbook of Optics*, (McGraw-Hill, New York, 1980).
13. H.E. Bennet, M. Silver, and E.J. Ashley, *J. Opt. Soc. Am.* **53** (1963) 1089.
14. V.I. Sapritsky *et al.*, *Proc. SPIE* **2815** (1996) 2.
15. F.O. Bartell and W.L. Wolfe, *Applied Optics* **15** (1976) 84.
16. A.J. LaRocca in "Artificial Sources", *The infrared handbook*, edited by W.L. Wolfe and G.J. Zissis, (ERIM, Ann Arbor, 1985).
17. V.I. Sapritsky and A.V. Prokhorov, *Applied Optics*. **34** (1995) 5645.
18. R. Siegel and J.R. Howell, *Thermal Radiation Heat Transfer*, (McGraw-Hill, New York, 1981).
19. E.M. Sparrow and R.D. Cess, *Radiation Heat Transfer*, (McGraw-Hill, New York, 1978).
20. H.C. Hottel and A.F. Sarofim, *Radiative Transfer*, (McGraw-Hill, New York, 1967).
21. F. Cabannes, *Propriétés Optiques à Haute Température, Facteurs D'Émission, International Flame Research Foundation*, (Ijmuiden, The Netherlands, 1975) Chap. 18.
22. T. Limperis in "Detectors", *The infrared handbook*, edited by W.L. Wolfe and G.J. Zissis, (ERIM, Ann Arbor, 1985).
23. G.J. Zissis in "Radiometry", *The infrared handbook*, edited by W.L. Wolfe and G.J. Zissis, (ERIM, Ann Arbor, 1985).
24. A.J. LaRocca in "Atmospheric Absorption", *The infrared handbook*, edited by W.L. Wolfe and G.J. Zissis, (ERIM, Ann Arbor, 1985).
25. ANSI MC 96.1 (1975).